THE JOURNAL OF BIOLOGICAL CHEMISTRY VOL. 289, NO. 42, pp. 29097–29111, October 17, 2014

Endocytosis of Secreted Carboxyl Ester Lipase in a Syndrome of Diabetes and Pancreatic Exocrine Dysfunction*

Received for publication, April 22, 2014, and in revised form, August 21, 2014 Published, JBC Papers in Press, August 25, 2014, DOI 10.1074/jbc.M114.574244

Janniche Torsvik[‡§1], Bente B. Johansson[‡§1], Monica Dalva[‡§¶], Michaël Marie[‖], Karianne Fjeld[‡§], Stefan Johansson[‡§], Geir Bjørkøy[‡‡], Jaakko Saraste[‖], Pål R. Njølstad[‡§§], and Anders Molven[‡¶¶2]**

From the [‡]KG Jebsen Center for Diabetes Research, Department of Clinical Science, University of Bergen, Bergen, Norway, [§]Center for Medical Genetics and Molecular Medicine, Haukeland University Hospital, Bergen, Norway, [¶]Gade Laboratory for Pathology, Department of Clinical Medicine, University of Bergen, N-5021 Bergen, Norway, [‖]Department of Biomedicine and Molecular Imaging Center, University of Bergen, Bergen, Norway, [**]Department of Technology, University College of Sør-Trøndelag, Trondheim, Norway, [‡‡]Centre of Molecular Inflammation Research, Department of Cancer Research and Molecular Medicine, Norwegian University of Science and Technology, Trondheim, Norway, [§§]Department of Pediatrics, Haukeland University Hospital, Bergen, Norway, and [¶¶]Department of Pathology, Haukeland University Hospital, Bergen, Norway

Background: Mutations in the carboxyl ester lipase (*CEL*) gene cause a syndrome of pancreatic exocrine and endocrine dysfunction (MODY8).
Results: Secreted mutant CEL forms aggregates that line the plasma membrane and are cleared by endocytosis.
Conclusion: The mutant and normal CEL protein exhibit different cellular properties both in pancreatic and non-pancreatic cell models.
Significance: MODY8 pathogenesis may involve endocytosis of a mutant CEL protein with toxic effect.

Maturity-onset diabetes of the young, type 8 (MODY8) is characterized by a syndrome of autosomal dominantly inherited diabetes and exocrine pancreatic dysfunction. It is caused by deletion mutations in the last exon of the carboxyl ester lipase (*CEL*) gene, resulting in a CEL protein with increased tendency to aggregate. In this study we investigated the intracellular distribution of the wild type (WT) and mutant (MUT) CEL proteins in cellular models. We found that both CEL-WT and CEL-MUT were secreted via the endoplasmic reticulum and Golgi compartments. However, their subcellular distributions differed, as only CEL-MUT was observed as an aggregate at the cell surface and inside large cytoplasmic vacuoles. Many of the vacuoles were identified as components of the endosomal system, and after its secretion, the mutant CEL protein was re-internalized, transported to the lysosomes, and degraded. Internalization of CEL-MUT also led to reduced viability of pancreatic acinar and beta cells. These findings may have implications for the understanding of how the acinar-specific CEL-MUT protein causes both exocrine and endocrine pancreatic disease.

The carboxyl ester lipase (*CEL*)[3] gene encodes carboxyl ester lipase, also known as bile salt-stimulated or -dependent lipase, which is highly expressed in pancreatic acinar cells. The CEL protein is one of three major lipases secreted from the exocrine pancreas into the pancreatic juice (1–3). In addition, a high level of *CEL* expression is found in lactating mammary glands where the enzyme is secreted as a component of breast milk (4). CEL is activated by bile salts and promotes absorption of cholesteryl esters from the small intestine by hydrolyzing them into free cholesterol and fatty acids (5). The enzyme also hydrolyzes fat-soluble vitamins (2) and triglycerides (6). Pancreatic CEL is transported from the duodenum via enterocytes to the blood (7), where it associates with low density lipoprotein (8). The protein is cleared from the circulation by renal glomerulus filtration and can be detected in the urine of healthy individuals (9).

CEL is kept in close proximity to intracellular membranes during its transport from the endoplasmic reticulum (ER) to post-Golgi compartments in the acinar cells (10). Its membrane association is due to an interaction with a multiprotein complex that contains the chaperone GRP94 (glucose-regulated protein of 94 kDa) (11, 12). CEL is co-translationally *N*-glycosylated at amino acid residue Asn-210 in the rough ER (13) followed by *O*-glycosylation at sites located in a variable number of tandem repeats (VNTR) present in the C-terminal domain of the protein (14). *O*-Glycosylation has been suggested to protect the protein against intracellular degradation by masking PEST sequences (15). It has also been shown to reduce proteolytic degradation of the secreted enzyme in the duodenum (16). Moreover, *O*-glycosylation could be important for the solubility of the protein, protecting against self-association caused by exposed hydrophobic surfaces on the globular core of the enzyme (17). In the trans-Golgi area, phosphorylation releases CEL from the multiprotein folding complex, and the protein is concentrated and stored in zymogen granules before its secretion to the cell exterior upon stimulation (18).

* This work was supported by grants from the Translational Fund of the Bergen Medical Research Foundation, the KG Jebsen Foundation, the University of Bergen, the Research Council of Norway, Haukeland University Hospital, Innovest, and the Western Norway Regional Health Authority (to A. M. and P. R. N.).
[1] Both authors contributed equally to the study.
[2] To whom correspondence should be addressed: Gade Laboratory for Pathology, Dept. of Clinical Medicine, University of Bergen, N-5021 Bergen, Norway. Tel.: 47-55973169; E-mail: anders.molven@gades.uib.no.
[3] The abbreviations used are: CEL, carboxyl ester lipase; ER, endoplasmic reticulum; GRP94, glucose-regulated protein of 94 kDa; IC, intermediate compartment; CHX, cycloheximide; BafA1, bafilomycin A1; MUT, mutant; MODY8, maturity-onset diabetes of the young, type 8.

The human *CEL* gene is highly polymorphic due to the VNTR in the last exon (19, 20). Each repeat encodes 11 amino acids, and the most common *CEL* allele in populations investigated so far contains 16 repeats (20–24). Single-base deletion mutations in the *CEL* VNTR have previously been shown to cause a syndrome of exocrine dysfunction and diabetes (named MODY8 (maturity-onset diabetes of the young, type 8) or *CEL*-MODY; OMIM #609812) in two Norwegian families (24). In the largest family a single-base deletion (c.1686delT) in the first repeat is predicted to lead to a frameshift that affects the next 111 amino acids, changing the C-terminal part of the enzyme. The resulting mutant protein is designated p.Val563CysfsX111 and will hereafter be referred to as CEL-MUT. Notably, the predicted VNTR of CEL-MUT differs in its amino acid composition compared with the VNTR of the normal protein (referred to as CEL-WT). CEL-MUT also lacks the 11 C-terminal amino acids tailing the CEL-WT VNTR.

It is still not understood why *CEL* VNTR mutations cause a dominantly inherited syndrome of exocrine and endocrine pancreatic dysfunction. Notably, lipomatosis of the pancreas is observed in the mutation carriers before disease is recognized at the clinical level (25). Because the *CEL* gene is not expressed in pancreatic beta cells, the negative effect of CEL-MUT on insulin secretion is likely to be secondary to a primary pathological event affecting the acinar cells. We previously reported that the changed C-terminal VNTR of CEL-MUT undergoes *O*-glycosylation and that the mutant protein is secreted to the cell exterior at a rate similar to what is seen for the WT when expressed in stably transfected HEK293 cells (26). Moreover, *in vivo* excreted CEL-MUT can be detected in pancreatic juice from the patients. Our findings led to the suggestion that CEL-MODY is a protein misfolding disease in which the CEL-MUT protein forms aggregates leading to the stimulation of the unfolded protein response (26).

The aim of the present study was to investigate whether the disease-causing c.1686delT mutation affects subcellular distribution, intracellular transport, and degradation of the CEL protein in cell line models. During these studies we discovered that there was a robust cellular reuptake of CEL-MUT after its secretion followed by transport to the lysosomes where the protein was degraded. Moreover, exposure to the CEL-MUT protein negatively affected the viability of pancreatic acinar and beta cells.

MATERIALS AND METHODS

Plasmids—cDNAs encoding wild type and mutant (c.1686delT/p.Val563CysfsX111) CEL were cloned into the pcDNA3.1/V5-His vector backbone (Invitrogen) in-frame with a C-terminal V5/His tag. This made it possible to detect the recombinant proteins by commercially available epitope-tag antibodies as well as with CEL-specific antibodies. The cloning procedure is described in detail in Johansson *et al.* (26). The CEL-WT construct has 16 repeated VNTR segments as in the most common allele found in Europeans (20, 22, 23, 24). In CEL-MUT, the single-base deletion located in the first repeat causes a frameshift and a premature stop codon. Thus, the translated CEL-MUT protein contains 11 repeated segments having a different amino acid composition than in the WT protein (24). We also constructed a plasmid expressing an artificial version of the CEL gene that lacked the sequence immediately after the mutated nucleotide (c.1686). The protein encoded by this plasmid was denoted CEL-TRUNC (p.Val563X) and only harbored the first four amino acids of the CEL VNTR region. CEL-TRUNC was employed to compare the effects caused by the altered VNTR seen in our patients to a situation where CEL is devoid of the VNTR. Plasmids encoding LC3-GFP and p62-mCherry have been described previously (27).

Antibodies and Reagents—Monoclonal (mAb) anti-V5 (R960-25), polyclonal anti-LAMP2 (51-2200), anti-mouse IgG-Alexa Fluor 488 (A11017), and anti-rabbit IgG-Alexa Fluor 594 (A11072) (both $F(ab)_2$-fragments) were purchased from Invitrogen. Anti-LAMP1 (sc-18821), horseradish peroxidase (HRP)-conjugated anti-actin (sc-8432 HRP), HRP-conjugated donkey anti-mouse (sc-2314), and HRP-conjugated anti-rabbit (sc-2313) were from Santa Cruz Biotechnology. Polyclonal anti-V5 (V8137) was from Sigma. Goat anti-mouse $F(ab)_2$-fragments coupled with HRP (BI3413C) were from PARIS Anticorps. Monoclonal antibody As20.1 and polyclonal antibody VANKO, both detecting CEL, were a generous gift from Dr. Olle Hernell (Department of Clinical Sciences, Umeå University, Umeå, Sweden). The polyclonal, rabbit antibody against GRP94 (affinity purified) was kindly provided by Dr. Linda Hendershot (St. Jude Children's Research Hospital, Memphis, TN). Monoclonal antibody detecting ERGIC-53/p58 (clone G1/93) was from Enzo Life Sciences, and monoclonal antibody directed against GM130 (610822) was from BD Transduction Laboratories. Rabbit antiserum against Rab1A was affinity-purified as described earlier (28). MG132 was obtained from Biomol. Cell growth medium, L-glutamine, cycloheximide, leupeptin, and phosphatase inhibitor mixture 2 were purchased from Sigma. Fetal bovine serum, penicillin-streptomycin, and Geneticin (G-418) were from Invitrogen. Epon 812 resin was from Electron Microscopy Sciences. The Enhanced Chemiluminescence (ECL) Plus Western blotting Detection kit was obtained from GE Healthcare, and FuGENE 6 transfection reagent and cOmplete Mini protease inhibitor mixture were from Roche Diagnostics. Total protein was measured using the BCA Protein Assay from Pierce.

Cell Culture, Transfection, and Drug Treatment—Human embryonic kidney (HEK) 293 cells (Clontech Laboratories), 266-6 cells (mouse pancreatic acinar cells, ATCC; CRL-2151), and HeLa cells (ATCC; CCL-2) were maintained in DMEM minimal essential growth medium (α-modification) supplemented with 10% fetal bovine serum, 100 units/ml penicillin-streptomycin, and 4 mM L-glutamine. Rat insulinoma INS 1E cells (a generous gift from Dr. Claes Wollheim, Geneva, Switzerland) were cultured in RPMI supplemented with 10% fetal bovine serum, 100 units/ml penicillin-streptomycin, 4 mM L-glutamine, 1% HEPES, and 1% sodium pyruvate. All cell cultures were maintained in 5% CO_2 at 37 °C.

HEK293 cells were transfected with pcDNA3.1/V5-His plasmids harboring *CEL*-WT, *CEL*-MUT, or *CEL*-TRUNC using FuGENE 6 as described by the manufacturer. Cells transfected with pcDNA3.1/V5-His without any insert (empty vector) were included in all experiments as a negative control. For stable CEL expression, transfected HEK293 cells were treated with 500 μg/ml Geneticin for 18 days followed by isolation of single cells. Clones showing similar levels of CEL-WT, CEL-MUT, and CEL-TRUNC mRNA and protein expression, as determined by

real-time quantitative PCR and Western blotting were chosen for further experiments.

HEK293 cells were treated with 1 μg/ml cycloheximide when investigating the rate of intracellular CEL clearance during inhibition of protein synthesis. In the proteasomal/lysosomal and autophagic degradation experiments, cells were incubated with 10 μM MG132, 100 μg/ml leupeptin, or 100 nM bafilomycin A1 for 3 h before fixation.

SDS-PAGE and Western Blotting—Cells were lysed in buffer containing 50 mM Tris (pH 8), 150 mM NaCl, 0.5% deoxycholate, 1% Nonidet P-40 and 1x Complete Mini protease inhibitor mixture. After centrifugation at 14,000 $\times$ *g* for 5 min, the supernatant was separated by SDS-PAGE (4–12%) and transferred to a PVDF membrane by standard methods. The pellet fraction was added sample buffer and boiled before gel electrophoresis. The proteins of interest were detected using specific antibodies and visualized by enhanced chemiluminescence. The membranes were imaged on a LAS-1000 imager (Fujifilm), and quantification of protein bands was performed using the Image Gauge v4.0 software (Fujifilm).

Immunostaining and Confocal Microscopy—Cells grown on poly-L-lysine-coated glass coverslips were fixed for 30 min with 3% paraformaldehyde and immunostained as described in Sannerud *et al.* (29). The coverslips were mounted in Gold Antifade Solution with DAPI from Invitrogen. Images were collected using a TCS SP2 or SP5 AOBS confocal microscope (Leica Microsystems) with 63×/1.4 NA and 100×/1.4 NA HCX Plan-Apochromat oil immersion objectives, ~1.2 airy unit pinhole aperture, and appropriate filter combinations. Images were acquired with 405 diode and argon ion/argon krypton lasers (Leica). Series of images were acquired at 0.19-μm intervals throughout the entire depth of the cells. The obtained images were processed using Photoshop CS4 and CS5 imaging software and illustrator CS6 (Adobe Systems).

Immunoperoxidase Electron Microscopy—Stably transfected HEK293 cells cultured on plastic culture dishes coated with poly-L-lysine were grown to a confluency of 70–80%, washed with PBS, and fixed with periodate/lysine/paraformaldehyde fixative (30). The pre-embedding immunoperoxidase procedure used for staining of cells with affinity-purified monoclonal antibodies against CEL (As 20.1) and goat anti-mouse $F(ab)_2$-fragment-coupled HRP has been described in detail elsewhere (31). Thin sections of the immunolabeled cells embedded in Epon 812 resin were stained with lead citrate and examined in a JEOL 1230 electron microscope (JEOL) operated at 60 kV.

Cell Fractionation—Velocity sedimentation of 3000 $\times$ *g* supernatants prepared from HEK293 cells in iodixanol gradients (Optiprep) was carried out as described previously (29). Briefly, HEK293 cells were cultured in flasks until they reached 80–90% confluency. The cells were washed, harvested in Hanks' balanced salt solution, and concentrated by centrifugation at 300 $\times$ *g*. The cell pellets were resuspended in ice-cold homogenization solution (130 mM KCl, 25 mM NaCl, 1 mM EGTA, 25 mM Tris-HCl (pH 7.4)) supplemented with 1× Complete Mini protease inhibitor mixture, and homogenized by 20 passages through a ball-bearing cell cracker (EMBL) with a clearance set at 0.01 mm. The extent of cell breakage was checked by phase contrast microscopy. The samples obtained after velocity sedimentation were separated using 10% SDS-PAGE and subjected to Western blotting.

Treatment with Conditioned Media—HEK293 cells stably expressing CEL protein variants were grown for 24 h toward confluence. The conditioned media were filtered (0.4 μm) to remove detached and dead cells and added to untransfected HEK293, HeLa, 266-6, or INS 1E cells for various time points as indicated under "Results." Immunostaining and confocal microscopy were then performed as described above.

Cell Viability—Cell viability was monitored by quantitation of ATP generated by metabolically active cells. The assay was performed using a CellTiter Glo luminescent cell viability kit (Promega) according to the manufacturer's instructions. Briefly, 5×10^2 266-6 cells and 5×10^3 INS 1E cells were seeded in sterile 96-well plates and grown in the conditioned medium for 7 days. CellTiter Glo reagent (100 μl) was added to lyse the cells. After 30 min of incubation at room temperature, 2 min of shaking, and 10 min of stabilization, the luminescence was recorded in a Tecan Infinite M200PRO luminometer with an integration time of 1 s per well. Four independent experiments, each consisting of 12 parallels, were conducted.

Apoptosis Assay—266-6 and INS 1E cells were seeded to a density of 2×10^5 cells/well on coverslips in 12-well plates and grown for 7 days in conditioned culture media. Caspase-3/7 enzymatic activity levels were measured using the CellEVENT Caspase-3/7 Green detection reagent (Invitrogen) according to the manufacturer's instructions. Briefly, detection reagent was added to the cell cultures to a final concentration of 7.5 μM and incubated for 30 min at 37 °C. The growth medium was removed, and the cells were fixed in 3% paraformaldehyde solution. Confocal microscopy was then performed as described above. The apoptosis assay was repeated three times with similar results.

RESULTS

Intracellular Distribution of CEL Is Strongly Affected by the c.1686delT Mutation—We previously established a HEK293 cell culture model that stably expresses CEL-WT and CEL-MUT (26). Here we have employed the model to investigate the intracellular distribution of the two CEL variants. Immunofluorescence staining followed by confocal microscopy showed that CEL-WT displayed the typical intracellular distribution of a secreted protein, including localization to a widespread ER-like reticular network and accumulation in the juxtanuclear Golgi area (Fig. 1*A*), consistent with previous results on the localization of CEL in human acinar cells (32). Interestingly, the intracellular localization of CEL-MUT differed considerably from that of the WT protein (Fig. 1, *B* and *C*). Screening of a large number of CEL-MUT-expressing cells revealed two major subpopulations with distinct fluorescence patterns. The cells in the first category, accounting for 53% of the MUT population (denoted *MUT #1*; Fig. 1*B*), typically displayed perinuclear puncta of variable size in addition to an intensive juxtanuclear Golgi-like staining. In the remaining 47% of the cells the punctate structures were much more numerous and widespread, whereas the Golgi- and ER-like signals appeared relatively weak (*MUT #2*; Fig. 1*C*).

We also tested a truncated variant of CEL, CEL-TRUNC (p.Val563X), where the introduction of a stop codon immedi-

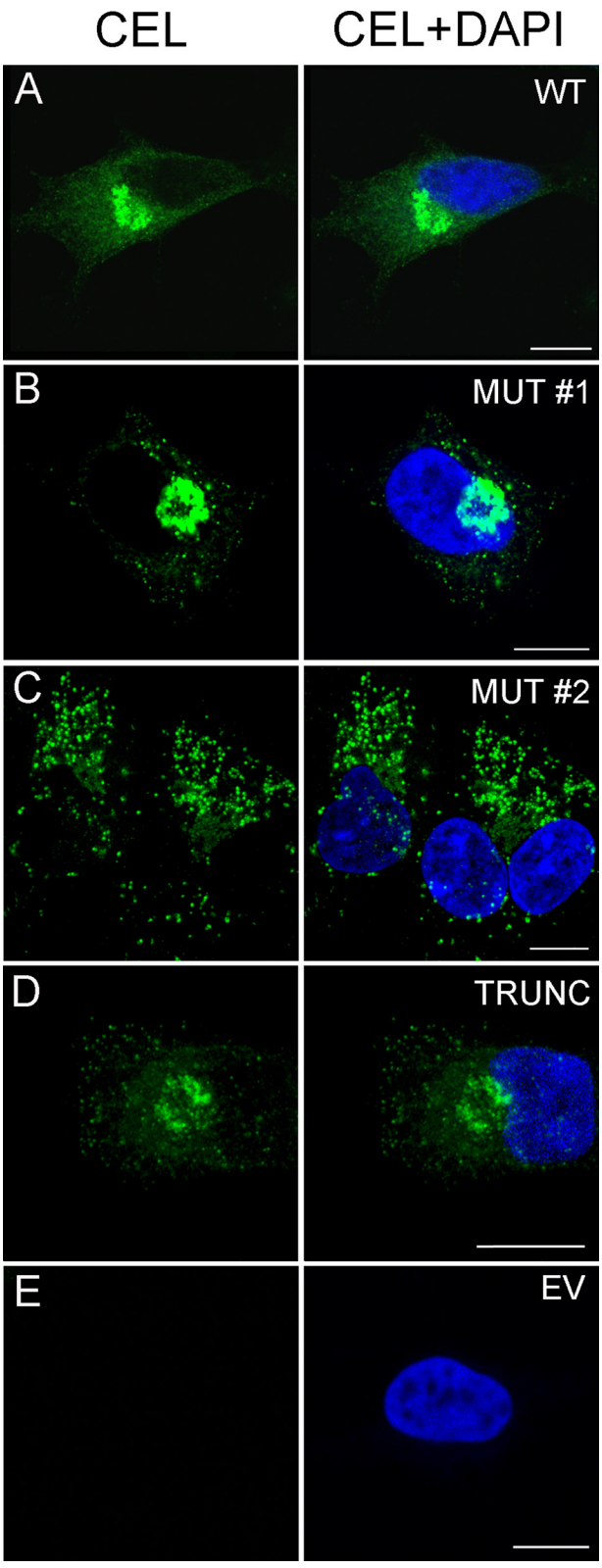

FIGURE 1. **Intracellular distribution of CEL protein variants.** *A*, stably transfected HEK293 cells expressing the three different CEL variants were stained using the anti-CEL antibody As20.1 and analyzed by confocal microscopy. The CEL-WT protein localized to the widespread reticular ER and also accumulated in the Golgi region. *B*, cells expressing CEL-MUT displayed two distinct localization patterns (scored in >600 cells). In the first population CEL-MUT was present in relatively small cytoplasmic punctate structures as well as in the Golgi compartment (MUT #1). *C*, in the remaining cells *(MUT #2)* the protein accumulated in somewhat larger and more intensely stained bodies dispersed throughout the cytoplasm. *D*, cells expressing CEL-TRUNC had an intracellular distribution pattern intermediate of WT and MUT #1, as the protein showed ER staining and accumulation in the perinuclear Golgi region (seen in WT), but also accumulated in small cytoplasmic bodies similar to MUT #1. *E*, untransfected HEK293 cells did not show any CEL-specific staining. Images represent maximum intensity projections of z-stacks taken through the entire depth of the cells. *Scale bars* represent 10 μm. *EV*, empty vector.

ately after the deleted nucleotide of CEL-MUT (c.1686) results in a complete loss of the VNTR after the mutation site. Also CEL-TRUNC was detected in punctate structures (Fig. 1*D*), but these were smaller and did not stain so intensively as the structures seen in MUT-expressing cells. In addition, variable Golgi-like staining resembling the MUT #1 pattern and diffuse ER-like staining similar to CEL-WT were observed in the cells expressing CEL-TRUNC. Untransfected HEK293 cells stained with the anti-CEL antibody did not exhibit any green fluorescence (Fig. 1*E*).

CEL-MUT Is Present in Intracellular Vacuoles and at the Plasma Membrane—Next, immunoperoxidase electron microscopy (EM) was carried out to analyze the subcellular localization of CEL-MUT at the ultrastructural level. The EM analysis revealed that the bright puncta detected in the MUT-expressing cells by confocal microscopy (Fig. 1, *B* and *C*) corresponded to vacuoles of variable size (0.5–1.0 μm in diameter). Some of the vacuoles were found as individual elements in the cytoplasm (Fig. 2*A*), whereas others associated with CEL-MUT-positive smooth membrane clusters (Fig. 2, *B* and *C*). Three types of vacuoles could be distinguished based on their size and internal distribution of the mutant protein. In the largest vacuoles (VAC1), CEL-MUT appeared to be tightly bound to the lumenal surface, whereas the rest of the lumen was devoid of the protein (Fig. 2*A*, *inset*). In other vacuoles (VAC2), the mutant protein did not associate with the limiting membrane but was distributed throughout the lumen (Fig. 2, *A* and *B*). Vacuoles of the third category (VAC3) were typically smaller and displayed patches of CEL-MUT along the lumenal surface (Fig. 2*C*, *inset*). Finally, extended aggregates of CEL-MUT were seen at the cell surface, most frequently at sites of close cell-to-cell contact (Fig. 2*A*, *inset*).

CEL-WT and CEL-MUT Co-distribute with Markers of the Early Secretory Pathway—We previously reported that secretion of both CEL-WT and CEL-MUT from HEK293 cells occurs at similar rates (26). However, the microscopic data described above indicated that the two proteins display clearly distinct intracellular distributions (Fig. 1, *B* and *C*; Fig. 2). To further compare the distributions of the two CEL variants along the secretory pathway, we employed cell fractionation (Fig. 3). Post-mitochondrial supernatants were prepared from HEK293 cells expressing CEL-WT or CEL-MUT and subjected to velocity sedimentation in iodixanol gradients (29). Thereafter, the distribution of CEL in gradient fractions were compared with different markers residing in the early secretory compartments, including GRP94 (ER), p58 (ER, intermediate compartment (IC), *cis*-Golgi), Rab1 (IC, *cis*-Golgi), and GM130 (IC, *cis*-Golgi). As shown in Fig. 3, the mature *O*-glycosylated, high molecular weight forms of both CEL-WT and CEL-MUT were predominantly detected in the slowly sedimenting post-ER membranes (fractions 2 and 3) co-distributing with IC/*cis*-

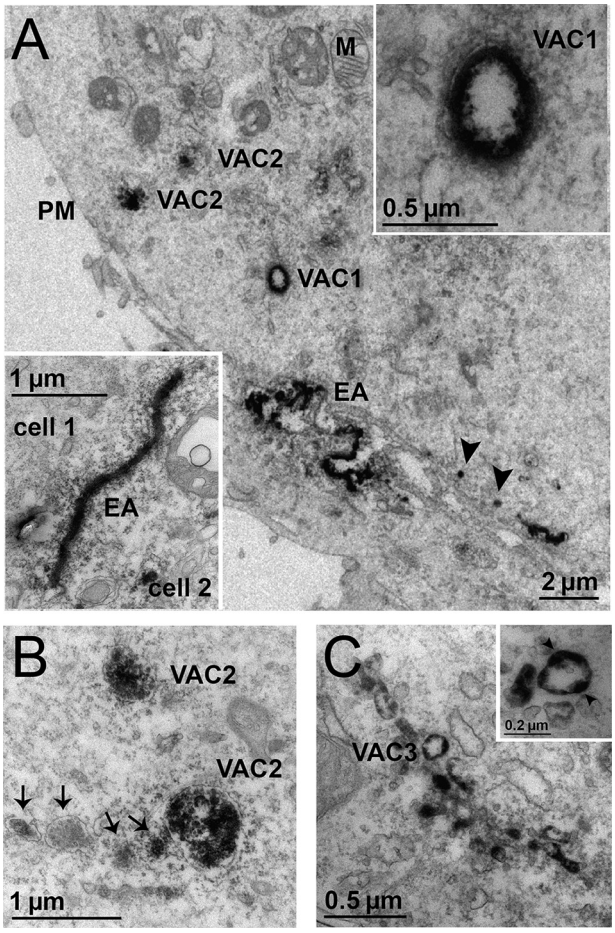

FIGURE 2. **Accumulation and aggregation of CEL-MUT.** *A*, stably transfected HEK293 cells were processed for immunoperoxidase electron microscopy using the anti-CEL antibody As20.1. Elongated CEL-MUT aggregates were seen outside the cells either aligning with free cell surface or residing at the narrow space between two adjacent cells (*inset*). Three different types of vacuoles were observed intracellularly. VAC1 were large vacuoles in which the mutant protein associated with the inner surface of the limiting membrane (*A* and *inset*). *Arrowheads* indicate small CEL-containing vesicles. *B*, in another class of large vacuoles (*VAC2*), CEL-MUT aggregates were present throughout the whole lumen. The *arrows* indicate smaller vacuoles that were negative or weakly positive for CEL-MUT. *C*, CEL-MUT was also frequently found associated with smaller pleomorphic (vacuolar) structures (*VAC3*) in which the protein was present in patches lining the inner membrane. *EA*, extracellular aggregates; *M*, mitochondrion; *PM*, plasma membrane; *VAC*, vacuole.

Golgi markers Rab1, p58, and GM130. Another peak of mature CEL-MUT, but only relatively small amounts of mature CEL-WT, was detected in faster sedimenting post-ER fraction (fraction 5). This pool of CEL-MUT could correspond to the smallest vacuolar structures (VAC3; Fig. 2*C*), which resemble pleomorphic IC elements in their morphology and sedimentation behavior (28, 33). The immature, low molecular weight forms of both CEL variants co-distributed with a minor pool of p58 in the fast-sedimenting ER factions (fractions 6–9). Moreover, they co-distributed with the ER chaperone GRP94 in agreement with the previously reported association of CEL with a GRP94-containing, membrane-bound, multiprotein folding complex (10, 32). The somewhat wider distribution profile of CEL-MUT could indicate that this protein was more prone to associate with membranes intracellularly as well as extracellularly (Fig. 2*A*; Ref. 26).

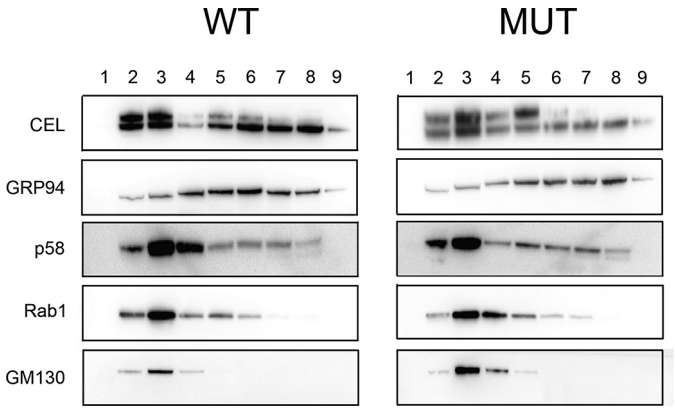

FIGURE 3. **Distribution of CEL-WT and CEL-MUT in the early secretory pathway analyzed by cell fractionation.** A 3000 × *g* supernatant prepared from HEK293 cells stably expressing CEL-WT or CEL-MUT was subjected to velocity sedimentation in a 5–25% iodixanol gradient. Nine fractions (*lanes 1–9*) were collected and subjected to SDS-PAGE followed by immunoblotting with antibodies detecting CEL (anti-V5) or different protein markers of early secretory compartments (GRP94, p58/ERGIC-53, Rab1, GM130). The data are representative of three experiments giving similar results.

Increased Stability of CEL-MUT upon Cycloheximide (CHX) Treatment—Some of the vacuoles seen in CEL-MUT-expressing cells might be related to post-Golgi steps in the secretion of the protein. We, therefore, treated cells with CHX to examine whether these vacuoles would disappear as a consequence of the inhibition of protein synthesis. Confocal microscopy showed that in cells expressing CEL-WT, the intensity of CEL-specific fluorescence decreased considerably after 60 min of CHX treatment (Fig. 4*A*). After 90 min the cells appeared almost devoid of the protein. A reduction of CEL-specific fluorescence was seen also in the CEL-MUT-expressing cells, but 90 min after the cessation of protein synthesis the amount of intracellular CEL-MUT protein was considerably higher than that of CEL-WT (Fig. 4*A*). The mutant protein was mainly localized in punctate structures corresponding to the vacuoles described above (Fig. 2). Western blotting of the detergent-soluble fractions of the total cell lysates showed that the intracellular pools of the soluble forms of the two CEL variants decreased at similar rates when protein synthesis was blocked (Fig. 4*B*). After 90 min of treatment with CHX, ~7% of the original pools remained for both protein variants (Fig. 4*C*). However, similar analysis of the pelleted material revealed the presence of a significant amount of CEL-MUT in this fraction. The amount of pelleted CEL-MUT decreased with increasing CHX exposure (Fig. 4*B*) but at a slower rate compared with the detergent-soluble fraction, and after 90 min of treatment ~20% of the protein remained (Fig. 4*C*). The punctate structures (vacuoles) seen in CEL-MUT-expressing cells after a 90-min CHX incubation could, therefore, represent an aggregated, Nonidet P-40-insoluble form of the mutant protein that had a longer half-life than the soluble form.

CEL-MUT Associates with LAMP1-positive Membranes—Because the majority of the vacuoles containing CEL-MUT could not be linked to protein secretion, we wondered whether they might be involved in protein degradation. Intracellular proteins can be degraded by two different mechanisms. The proteasome is responsible for degrading short-lived, soluble proteins (34), whereas autophagy is a degradation pathway that delivers long-lived proteins, protein aggregates, and organelles

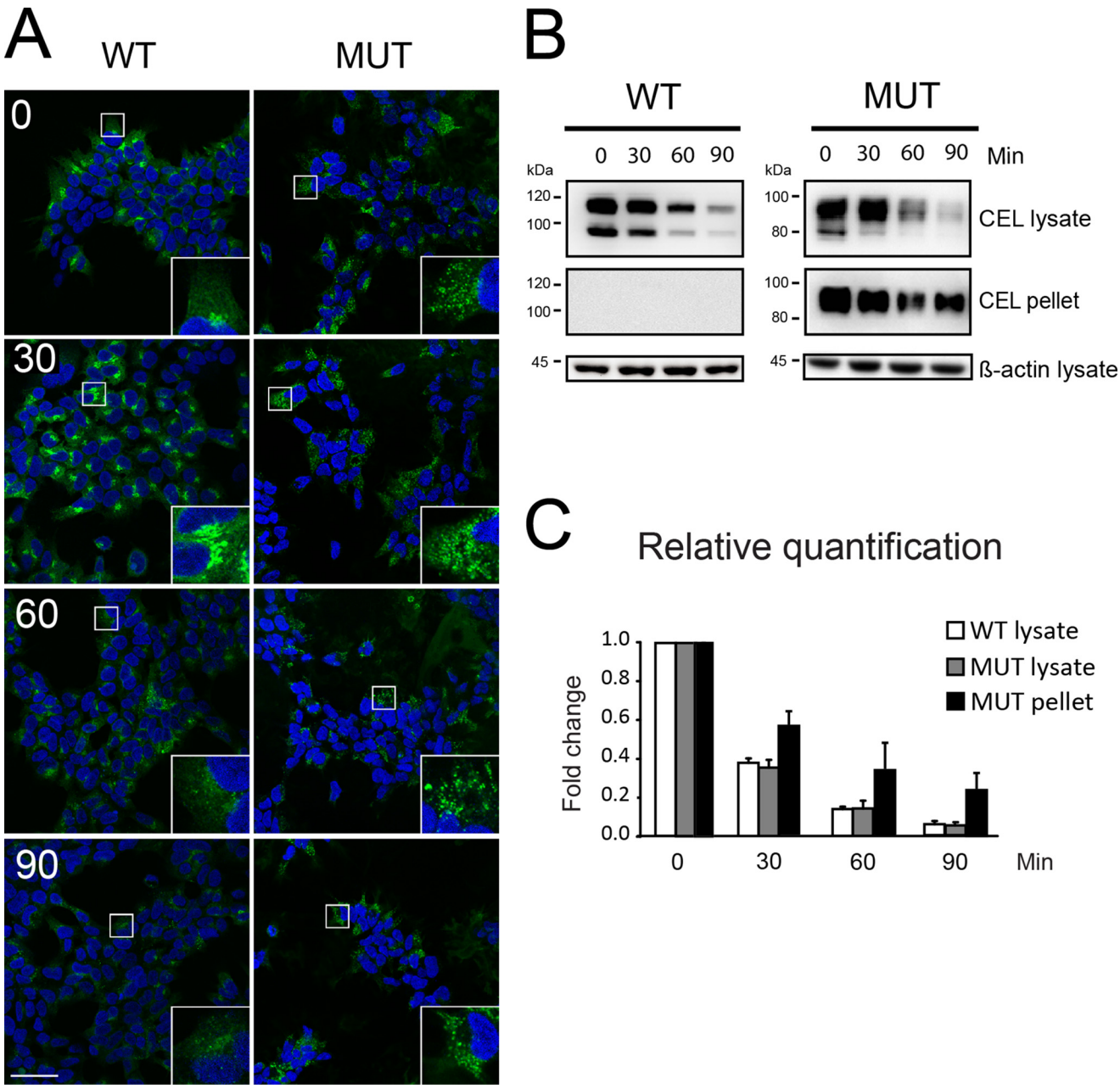

FIGURE 4. **Reduced cellular clearance of CEL-MUT upon cycloheximide treatment.** *A*, stably transfected HEK293 cells were treated with 1 μg/ml cycloheximide. The intracellular levels of protein were monitored by confocal microscopy in 30-min intervals (image labels) after the addition of cycloheximide. The cells were stained with the anti-CEL antibody As20.1. Images were obtained using confocal microscopy with identical laser and microscope settings. Each image represents maximum intensity projections of a z-stack taken through the entire depth of the cells. The *scale bar* represents 50 μm. *B*, HEK293 cells treated as in *A* were lysed and centrifuged for 10 min at 3000 $\times$ *g*. The resulting supernatant fractions and the pelleted membrane fractions were analyzed by Western blotting using an anti-V5 antibody. *C*, the bands in *B* were quantified and normalized to the β-actin level. CEL concentration at 0 min was arbitrarily set to 1.0, and relative CEL concentrations at other time points are shown. Data are shown as the means; the *error bar* represents S.D. from three independent experiments, each consisting of three parallels.

to the lysosomes where they are eliminated (35). The localization of CEL-MUT to large vacuolar structures suggested an association with lysosomes. We, therefore, co-stained CEL-WT-, CEL-MUT-, and CEL-TRUNC-expressing HEK293 cells with antibodies against CEL and LAMP1, a membrane protein present in late endosomes and lysosomes (36). Only 2% of WT-expressing cells displayed co-localization between LAMP1 and CEL, whereas ~30% of MUT-expressing cells showed CEL-positive vacuoles surrounded by LAMP1-positive membranes (Fig. 5, *A* and *C*). Notably, also 17% of the untreated CEL-TRUNC-expressing cells displayed co-localization between LAMP1 and CEL, a number intermediate of WT and MUT cells (Fig. 5, *A* and *C*).

We next investigated the effect on the formation of the vacuolar structures of the drug leupeptin, an inhibitor of serine and cysteine proteases found in the lysosomes, and of MG132, an inhibitor of both the proteasome and certain lysosomal cysteine proteases (37). After a 3-h leupeptin treatment, 76% of the cells expressing CEL-MUT exhibited LAMP1/MUT double-positive vacuoles (Fig. 5, *A* and *C*), the average number of co-local-

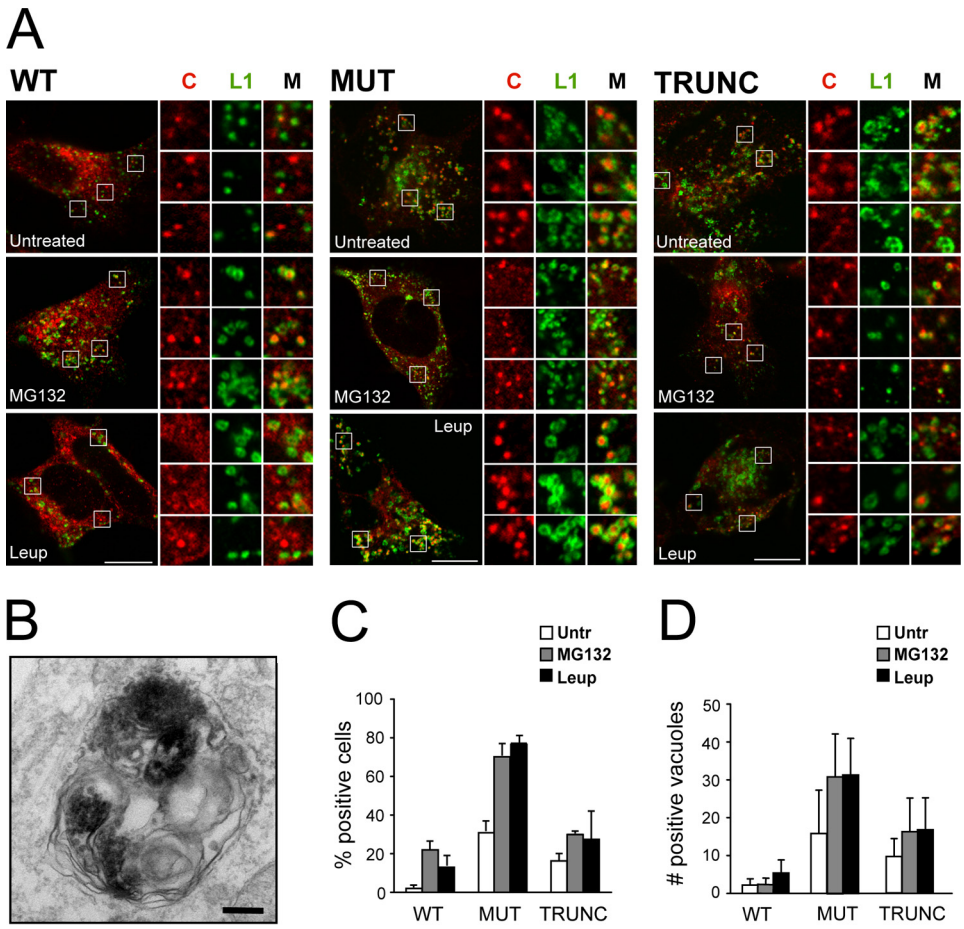

FIGURE 5. **Co-localization of CEL-MUT- and CEL-TRUNC-positive vacuoles with LAMP1.** *A*, stably transfected HEK293 cells were treated with vehicle (DMSO = untreated), 10 μM MG132, or 100 μg/ml leupeptin for 3 h. The cells were fixed and stained for CEL (VANKO antibody; *red*) and LAMP1 (*green*). Single confocal images are shown. *Scale bars* represent 10 μm. The *insets* show the *boxed areas* in additional 3.3× magnification. *B*, image from the electron microscope of a CEL-MUT-expressing cell after leupeptin treatment (As20.1 antibody). The *scale bar* represents 0.2 μm. *C*, diagram showing the percent of cells exhibiting co-localization between CEL and LAMP1 after different treatments. In total, 300 cells from three different experiments were analyzed. *D*, diagram showing the number of positive vacuoles counted in 40 cells from each treatment. Data are shown as the means; *error bars* represent S.D. from three independent experiments. *C*, CEL; *L1*, LAMP1; *M*, merge.

izing vacuoles in each positive cell being almost doubled (Fig. 5*D*). This confirmed that a substantial fraction of the MUT protein was transported to the lysosomes. Accordingly, immunoperoxidase EM showed that CEL-MUT was present in the lumen of lysosomal vesicles (Fig. 5*B*). A similar effect to that of leupeptin was seen after MG132 treatment (Fig. 5, *A*, *C*, and *D*).

In CEL-WT-expressing cells, the number of cells showing co-localization between LAMP1 and CEL increased to 13 and 22% after treatment with leupeptin and MG132, respectively (Fig. 5, *A* and *C*), but the number of positive structures within each positive cell remained relatively low (Fig. 5*D*). This indicated that the lysosomes are not a main degradation route of the WT protein. When CEL-TRUNC-expressing cells were exposed to MG132 and leupeptin, the fraction of cells showing co-localization between CEL and LAMP1 increased to 29 and 27%, respectively, a number intermediate of WT and MUT (Fig. 5, *C* and *D*).

Autophagy Is Not a Key Degradation Pathway of CEL-MUT—We previously found that CEL-MUT has an increased tendency to aggregate (26), and we therefore wanted to investigate if autophagy was involved in the delivery of the protein to the lysosomes. HEK293 cells stably expressing CEL-MUT were transiently transfected with a plasmid encoding LC3-GFP. The cells were then treated with bafilomycin A1 (BafA1) for 3 h, an antibiotic that blocks the fusion of autophagosomes and lysosomes and also inhibits lysosomal protein degradation. Confocal imaging showed that after BafA1 treatment, the number of CEL-MUT-containing vacuoles increased in both number and staining intensity, but no co-localization with LC3B was observed (Fig. 6*A*). As the number of LC3-positive vacuoles was quite low in HEK293 cells even after BafA1 treatment, we repeated the experiment in HeLa cells. The latter were transiently co-transfected with plasmids encoding CEL-MUT and LC3-GFP, and after 24 h a fraction of the HeLa cells was treated with BafA1 for 3 h before they were fixed and stained. Both autophagosomes and CEL-MUT-positive vacuoles were detected in the HeLa cells (Fig. 6*C*), but they did not co-localize, confirming that CEL-MUT was not transported to the lysosomes via the autophagosomal pathway.

Finally, we investigated if there was an association between CEL-MUT and p62, a protein known to bind to aggregated cytoplasmic proteins and mark them for autophagic degradation (27). HEK293 cells stably expressing CEL-MUT were tran-

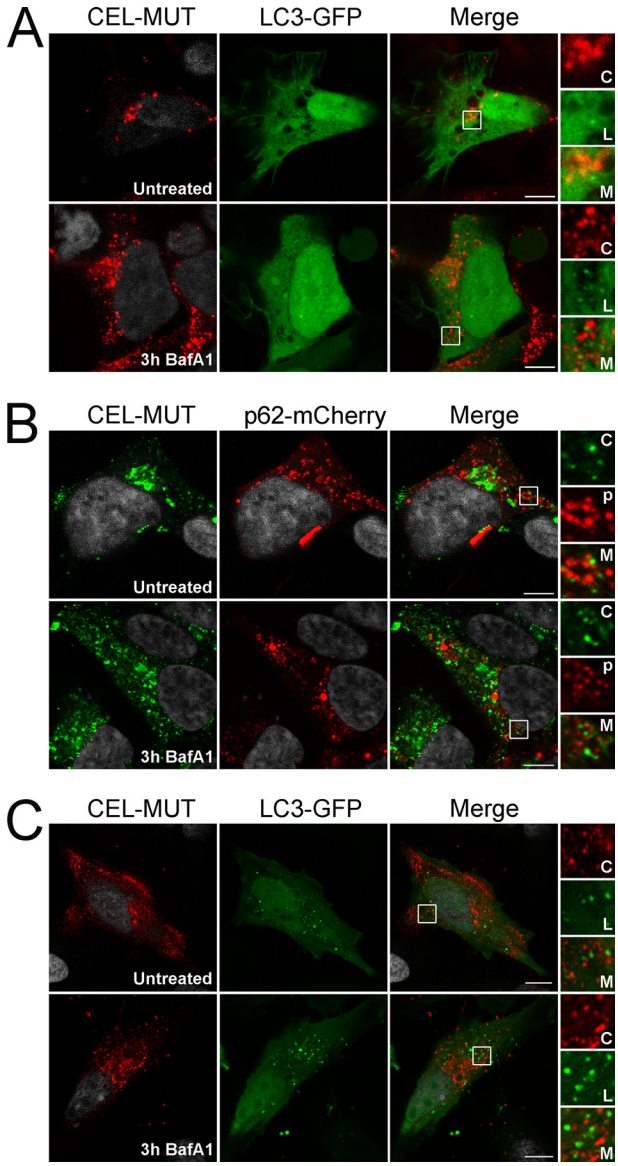

FIGURE 6. **CEL-MUT does not co-localize with autophagic markers.** *A*, HEK293 cells stably expressing CEL-MUT were transiently transfected with plasmids encoding LC3-GFP and treated with 100 nM BafA1 for 3 h. The cells were then fixed and stained using an anti-CEL antibody (As20.1). BafA1 treatment increased the intensity of CEL-MUT fluorescence and increased the number of MUT-positive vacuoles in the cells but did not result in a co-localization between CEL-MUT and LC3. *B*, HEK293 cells stably expressing CEL-MUT were transiently transfected with plasmids encoding p62-mCherry and treated as in *A*. No co-localization between CEL-MUT and p62-mCherry was observed before or after BafA1 treatment. *C*, HeLa cells were transiently co-transfected with plasmids encoding CEL-MUT and LC3-GFP and treated as in *A*. The LC3-positive puncta did not co-localize with CEL-MUT vacuoles before or after BafA1 treatment. Single confocal images are shown. *Scale bars* represent 10 μm, and *insets* represent an additional 3.3× magnification of the *boxed area*. *C*, CEL; *L*, LC3-GFP; *p*, p62-mCherry; *M*, merge.

siently transfected with a plasmid encoding p62-mCherry, grown for 24 h, and treated with BafA1 for the last 3 h before fixation. No co-localization could be seen between CEL-MUT and p62 either in untreated or in BafA1-treated cells (Fig. 6*B*). Taken together, our experiments could not detect degradation of CEL-MUT by autophagy, suggesting that the protein did not form insoluble aggregates during its synthesis but rather after its release to the cell exterior.

Secreted CEL-MUT Is Re-internalized via a Temperature-dependent Pathway—The lysosomes also represent the end point for endocytosis, a pathway that transports proteins from the cell exterior into the cell. As CEL-MUT was seen at the plasma membrane in distinct areas (Fig. 2) and inside lysosomal vacuoles (Fig. 5*A*) but not as part of the autophagosomal pathway (Fig. 6), we investigated whether the MUT-positive vacuoles resulted from re-uptake of the secreted protein. Untransfected HEK293 cells, which do not express endogenous CEL, were incubated for 24 h in conditioned medium from stably transfected HEK293 cells expressing CEL-WT, CEL-MUT, or CEL-TRUNC. A fraction of the cells were also incubated with leupeptin for the last 3 h. Confocal microscopy of immunostained cells showed that in ~20% of WT-exposed cells, the protein could be seen intracellularly (Fig. 7, *A* and *B*). Leupeptin treatment did not increase the intensity of the CEL-WT-specific staining. In contrast, CEL-MUT was seen intracellularly in ~90% of the HEK293 cells exposed to CEL-MUT-conditioned medium, and after leupeptin treatment, CEL-specific fluorescence increased significantly (Fig. 7, *A* and *B*), showing that CEL-MUT from the cell exterior was transported to the lysosomes after being internalized. ~60% of the cells exposed to TRUNC medium were also positive, and a small increase in fluorescence intensity was seen in these cells after leupeptin treatment (Fig. 7, *A* and *B*).

To determine whether the transport of CEL into the cells was temperature-dependent, CEL-conditioned medium was added to untransfected HEK293 cells, which then were incubated at 4 °C or 37 °C for 30 min. Almost no endocytosis of either CEL variant could be observed after the 4 °C incubation (Fig. 7*B*). A similar experiment was then performed in HeLa cells exposed to the conditioned medium from CEL-expressing HEK293 cells as in Fig. 7*B*. The HeLa cells showed an efficient uptake of CEL-MUT and CEL-TRUNC when grown at 37 °C for 30 min (Fig. 7*C*), similar to the HEK293 cells (Fig. 7*B*). The HeLa cells were then exposed to the PI3K inhibitor wortmannin before and during incubation in CEL-containing medium. This resulted in strong inhibition of the endocytosis of both CEL-MUT and CEL-TRUNC, confirming that the mutant CEL proteins enter the cells through active transport (Fig. 7*C*). The latter experiment also showed that CEL-MUT can be produced and secreted from one cell line and be endocytosed by a different cell type.

CEL-MUT Is Rapidly Degraded in Lysosomes after Endocytosis in HeLa Cells—We then examined whether the three proteolysis inhibitors leupeptin, MG132, and BafA1 had a similar effect on the MUT-positive vacuoles resulting from endocytosis in HeLa cells as on the MUT vacuoles present in stably transfected HEK293 cells (Fig. 5). HeLa cells were grown in conditioned medium from HEK293 cells stably expressing CEL-MUT in the presence of the three inhibitors for 3 h, fixed, and stained using antibodies detecting CEL and LAMP1. Also in this experiment the internalized MUT protein accumulated in LAMP1-positive vacuoles after all three treatments (Fig. 8). Interestingly, also the proteasomal inhibitor MG132 caused accumulation of CEL inside LAMP1-positive structures in the HeLa cells, demonstrating that this inhibitor is not specific for the proteasome.

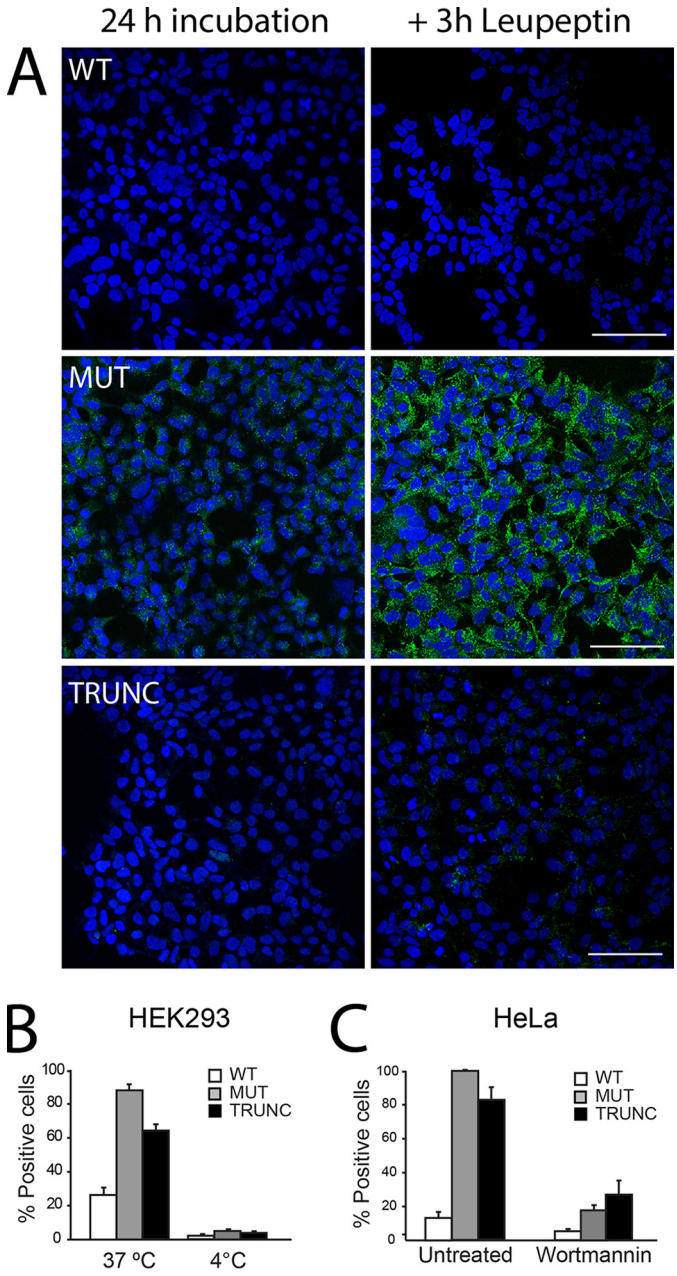

FIGURE 7. **Reabsorption of secreted CEL protein.** *A*, untransfected HEK293 cells were cultured in conditioned medium from HEK293 cells stably expressing CEL-WT, CEL-MUT, or CEL-TRUNC for 24 h. For the last 3 h a fraction of the cells was cultured in the presence of 100 μg/ml leupeptin. The cells were fixed and stained using the anti-CEL antibody As20.1. Each image represents a maximum intensity projection of a z-stack taken through the entire depth of the cells. The *scale bar* is 50 μm. *B*, untransfected HEK293 cells were preincubated at 37 or 4 °C for 15 min before the addition of 37 °C or ice-cold conditioned medium from cells expressing the three CEL variants and incubated for 30 min. The number of positive cells was quantified. *C*, untransfected HeLa cells were cultured in the presence of 100 nM wortmannin 20 min before and during incubation in conditioned medium (30 min). Both 4 °C incubation and wortmannin treatment partly blocked the internalization of CEL from the medium. Data in *B* and *C* are shown as the means, and *error bars* represent S.D. from three independent experiments where 100 cells were evaluated for each treatment.

Next, the kinetics of CEL-MUT internalization and degradation was investigated in HeLa cells. The cells were exposed to conditioned medium from HEK293 cells stably expressing CEL-MUT for 30 min. They were then washed with CEL-free growth medium and incubated for different time points followed by staining with antibodies detecting CEL-MUT and LAMP1 (Fig. 9). Intracellular MUT protein was seen at time 0, but most MUT-positive vacuoles did not co-localize with LAMP1 at this time point and, therefore, possibly represented early endosomes (Fig. 9*B*, *0 h*). However, 1 h after the conditioned medium had been removed, the majority of MUT-positive vacuoles co-localized with LAMP1, an association that continued for another hour. After 3 h, almost all CEL-MUT-specific staining had disappeared, indicating that CEL-MUT had been efficiently cleared by the lysosomes (Fig. 9*B*, *3 h*).

CEL-MUT Is Endocytosed Also by Pancreatic Acinar and Beta Cell Models—To investigate whether CEL-MUT could be endocytosed by pancreatic cells, mouse acinar cells (266-6) and rat insulinoma cells (INS 1E) were exposed for 30 min to conditioned medium from the HEK293 cells stably secreting CEL-MUT or CEL-WT, followed by fixation and immunostaining using CEL-specific antibodies. Confocal microscopy detected CEL-MUT in the cytoplasm of 90–100% of the 266-6 and INS 1E cells (Fig. 10, *B* and *D*), whereas CEL-WT was detected internally in only 10% of the cells (Fig. 10, *A* and *C*).

To investigate the mechanism and kinetics of internal CEL-MUT degradation in pancreatic cells, the same cell models were preincubated with conditioned medium from CEL-expressing HEK293 cells for 30 min, then washed with PBS and cultured in fresh medium for different time points before fixation. The fixed cells were immunostained for CEL as before, and lysosomes were stained using an antibody detecting the rodent LAMP2 protein. Immediately after removal of the conditioned medium, CEL-MUT was seen in vesicles in both cell models but did not co-localize with LAMP2-positive vesicles at this time point (Fig. 11, *A* and *B*, *0 h*). One hour after the medium change, vesicles positive for both CEL-MUT and LAMP2 were seen in 266-6 and INS 1E cells (Fig. 11, *A* and *B*), strongly suggesting that CEL-MUT was transported to the lysosomes in the two cell models similarly to what we had observed in HeLa and HEK293 cells (Figs. 5, 6, and 9). The CEL-MUT signal was lost 2 h after medium removal in the 266-6 cells, showing that CEL-MUT was rapidly degraded after it reached the lysosome in the acinar cell model (Fig. 11*A*). However, degradation of CEL-MUT was somewhat slower in the INS 1E cells as some co-localization persisted 2 h after medium removal (Fig. 11*B*).

Internalization of CEL-MUT Reduces the Viability of Pancreatic Acinar and Beta Cell Models—Finally, we investigated whether CEL protein internalization affected the viability of pancreatic cells. This experiment showed that cells exposed to conditioned media containing CEL-MUT produced a significantly lower level of ATP than cells cultured in the presence of CEL-WT, indicating that endocytosis of the mutant protein over time leads to a decrease in metabolic activity (Fig. 12*A*). The pancreatic cells were also examined for caspase-3/7 activity. Both 266-6 and INS 1E cells exposed to CEL-MUT exhibited clearly increased levels of active caspase-3/7 compared with cells exposed to CEL-WT (Fig. 12*B*). This indicated stimulation of apoptotic activity in pancreatic cells exposed to CEL-MUT confirming a possible toxic effect of the mutant protein.

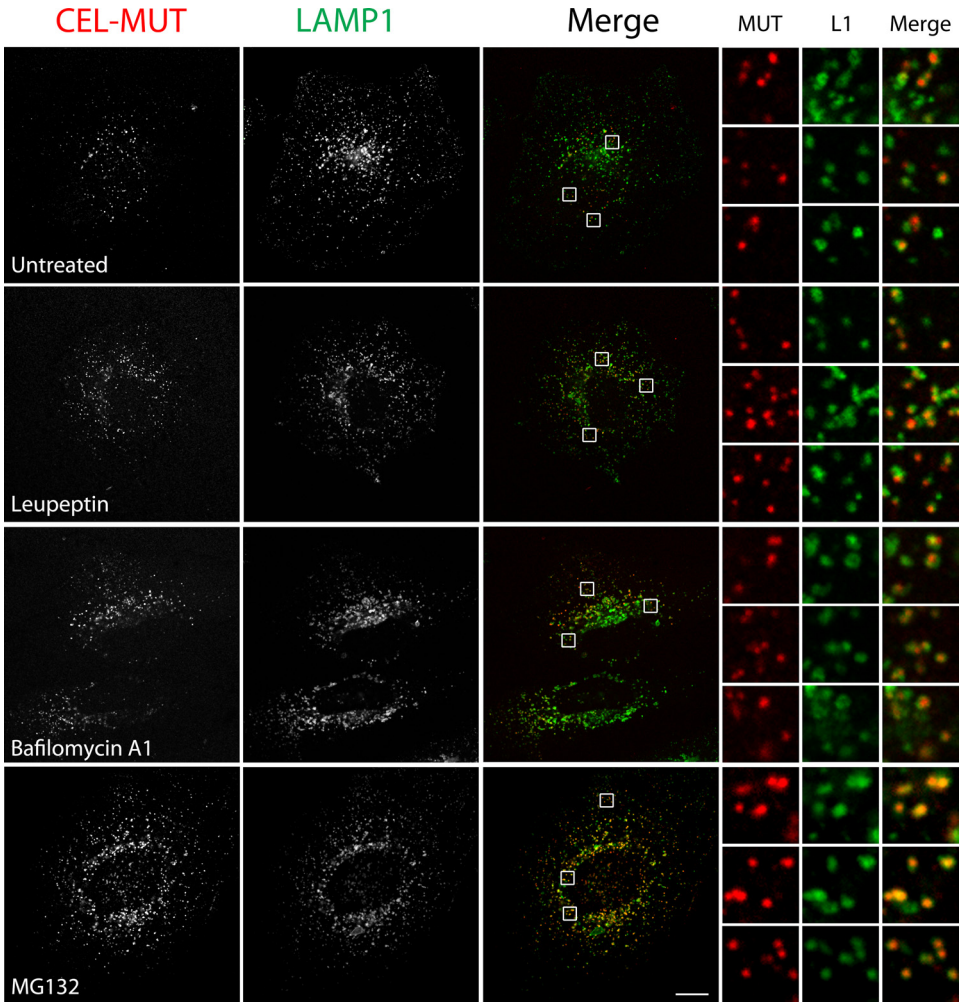

FIGURE 8. **CEL-MUT endocytosed by HeLa cells accumulates in LAMP1-positive vacuoles.** HeLa cells were cultured in conditioned medium from HEK293 cells stably expressing CEL-MUT for 3 h in the presence of vehicle (DMSO), 100 μg/ml leupeptin, 100 nM BafA1, or 10 μM MG132. After the treatments, the cells were fixed and stained using anti-CEL (VANKO; *red*) and anti-LAMP1 (*green*) antibodies. The *insets* show the *boxed areas* in additional 6.6× magnification. In untreated cells, only a fraction of the CEL-MUT vacuoles were LAMP1-positive, but after all three treatments most of the CEL-MUT-containing vacuoles localized to LAMP1-positive structures. Single confocal images are shown. The *scale bar* represents 10 μm. *L1*, LAMP1.

DISCUSSION

The aim of the present study was to elucidate the disease mechanism of CEL-MODY by investigating the intracellular distribution of the disease-causing protein in cell line models. We previously showed that CEL-MUT and CEL-WT exhibit similar patterns of post-translational modifications and rates of secretion but that CEL-MUT has a propensity to form aggregates (26). We, therefore, hypothesized that development of CEL-MODY might involve a gain-of-function effect conferred by the mutant protein, in accordance with the autosomal dominant inheritance pattern of the disease. Notably, studies of *Cel* knock-out mice have shown that these mice do not develop a pancreatic dysfunction, strongly supporting that loss of function alone is not causing the disease (38).

When observing the localization of three CEL protein variants in stably transfected cells by confocal microscopy, the most prominent difference was punctate, CEL-positive structures of variable size seen mainly in cells over-expressing CEL-MUT (Figs. 1 and 2). We confirmed that the mutant protein, but not the wild type or a truncated CEL variant lacking the VNTR, formed extracellular aggregates lining the outer surface of the plasma membrane. Moreover, experiments in cells that do not express any CEL protein showed that CEL-MUT presented extracellularly could be internalized via endocytosis and transported to the lysosomes where the protein is degraded.

Autophagy is a major protein degradation pathway in cells, and the final step of this process is the fusion of the autophagosome with lysosomes (35, 39). Clearance of CEL-MUT by autophagy might be expected, as this protein variant has the potential to form both soluble and insoluble aggregates (26). Moreover, increased eIF2α phosphorylation, which is seen in HEK293 cells expressing CEL-MUT (26), can promote degradation of protein aggregates by activating autophagy in addition to the role of eIF2α in the unfolded protein response (40). However, when we examined co-localization of CEL-MUT and LC3, a specific marker of the autophagosome, no overlapping distribution pattern was seen. We were also unable to detect co-localization between the mutant protein and p62, the latter being a protein that recruits the autophagic machinery to ubiquitinated protein aggregates and marks them for autophagic degradation (27, 41, 42). Aggregated CEL-MUT protein seems not to be ubiquitinated (26), and taken together, our data strongly

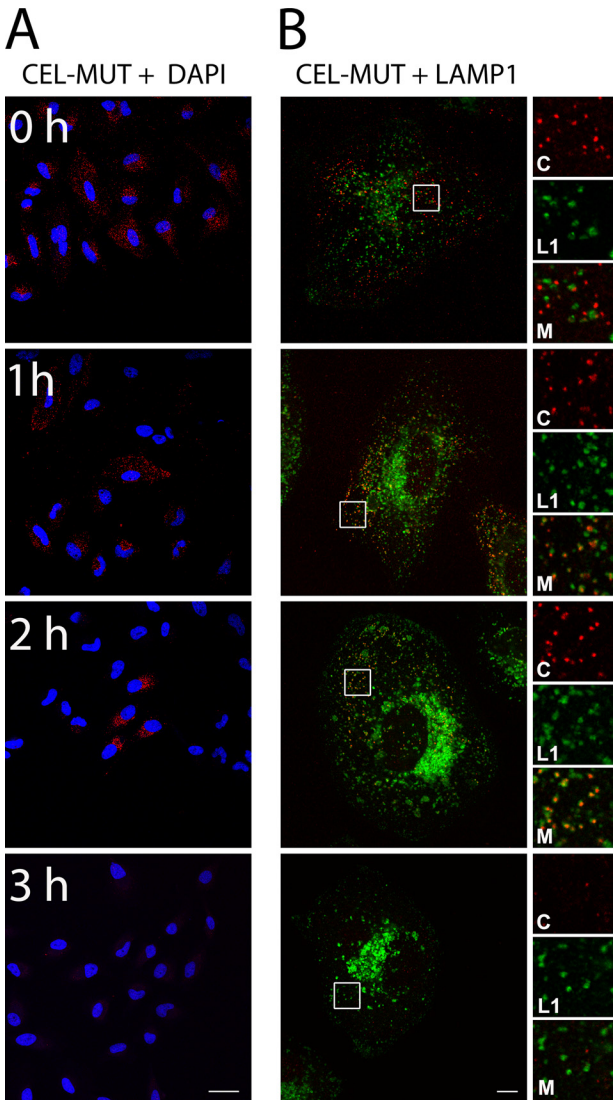

FIGURE 9. **Transport to lysosomes and rapid degradation of endocytosed CEL-MUT.** *A*, untransfected HeLa cells were cultured for 30 min in conditioned medium from HEK293 cells expressing CEL-MUT, washed 3 times with fresh medium, and incubated for the indicated time points (hours). The cells were fixed and stained using a polyclonal anti-CEL antibody (VANKO; *red*). Immediately after preincubation (*0 h*) CEL-MUT was seen inside most of the HeLa cells. Two hours after medium removal only a few cells remained positive, and after 3 h all cells were negative. Images are maximum intensity projections of a z-stack taken through the entire depth of the cells. The *scale bar* is 50 μm. *B*, HeLa cells were treated as in *A* and stained for CEL (VANKO antibody; *red*) and LAMP1 (*green*). At time 0 h, CEL was seen clustering in intracellular vesicles, but these did not co-localize with LAMP1. One hour after removal of the CEL-MUT medium a fraction of the CEL-positive vesicles co-localized with LAMP1, and after 2 h almost all CEL-containing vesicles detected were LAMP1-associated. Three hours after removal of the CEL medium the signal from CEL was lost, indicating that the protein was degraded when it reached the lysosomes. Single confocal images are shown. The *scale bar* is 10 μm. *C*, CEL; *L1*, LAMP1; *M*, merge.

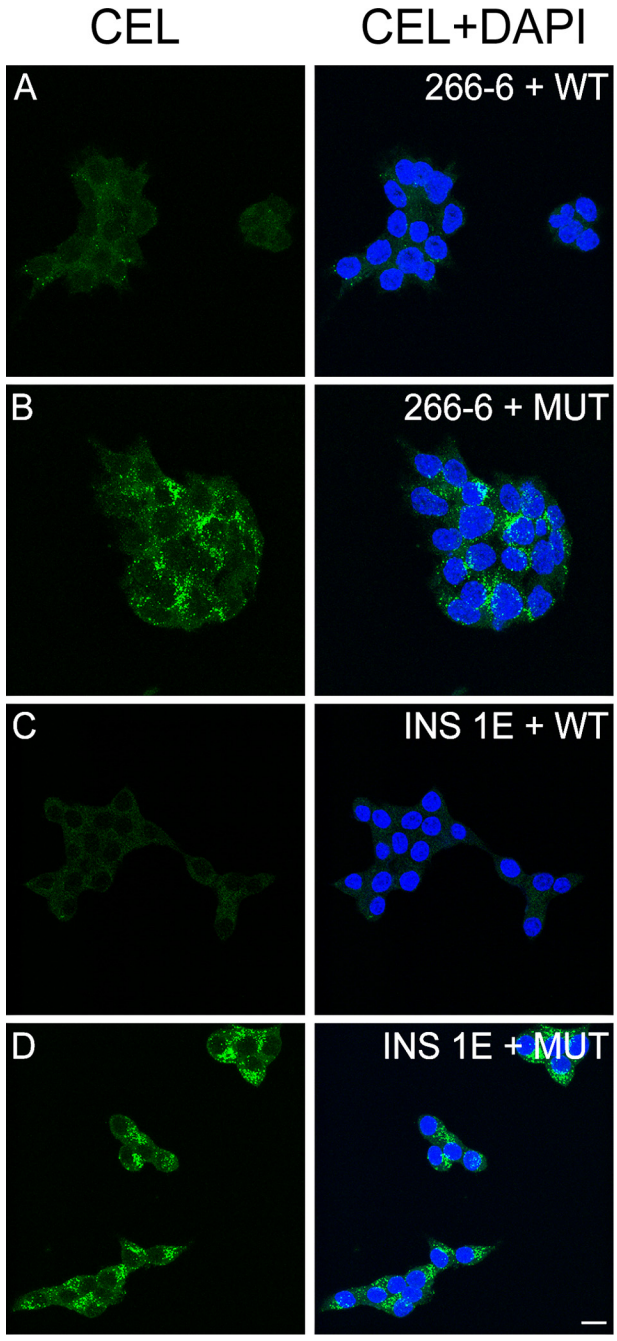

FIGURE 10. **Endocytosis of secreted CEL protein in pancreatic cells.** 266-6 (*A* and *B*) and INS 1E (*C* and *D*) cells were cultured for 30 min in conditioned medium from HEK293 cells stably expressing CEL-WT or CEL-MUT. The cells were fixed and stained using the anti-CEL antibody As20.1. Both 266-6 and INS 1E cells showed a higher propensity to endocytose CEL-MUT (90–100%) compared with CEL-WT (0–10%). Each image represents a maximum intensity projection of a z-stack taken through the entire depth of the cells. One hundred cells were counted in three independent experiments to establish the level of endocytosis for each CEL variant. The *scale bar* is 10 μm.

suggest that the majority of the mutant protein forms aggregates in the extracellular space after its secretion rather than within the cell during production and transport.

During this work, we made the new and intriguing observation of a strong cellular re-uptake of CEL-MUT by endocytosis, explaining the characteristic cellular phenotype shown in Fig. 1. We also found that the CEL-MUT protein secreted by stably transfected HEK293 cells could be endocytosed by three different human and rodent cell lines (HeLa, INS 1E, 266-6). Notably, the latter was a pancreatic acinar cell line demonstrating internalization in the cells where CEL is naturally produced. The observation of CEL-MUT endocytosis in the beta cell model INS 1E raises the possibility that in the CEL-MODY patients, pancreatic endocrine cells might take up the mutant protein if exposed to it.

The precise mechanism for how extracellular CEL-MUT is internalized by cells is still unknown, although our results sup-

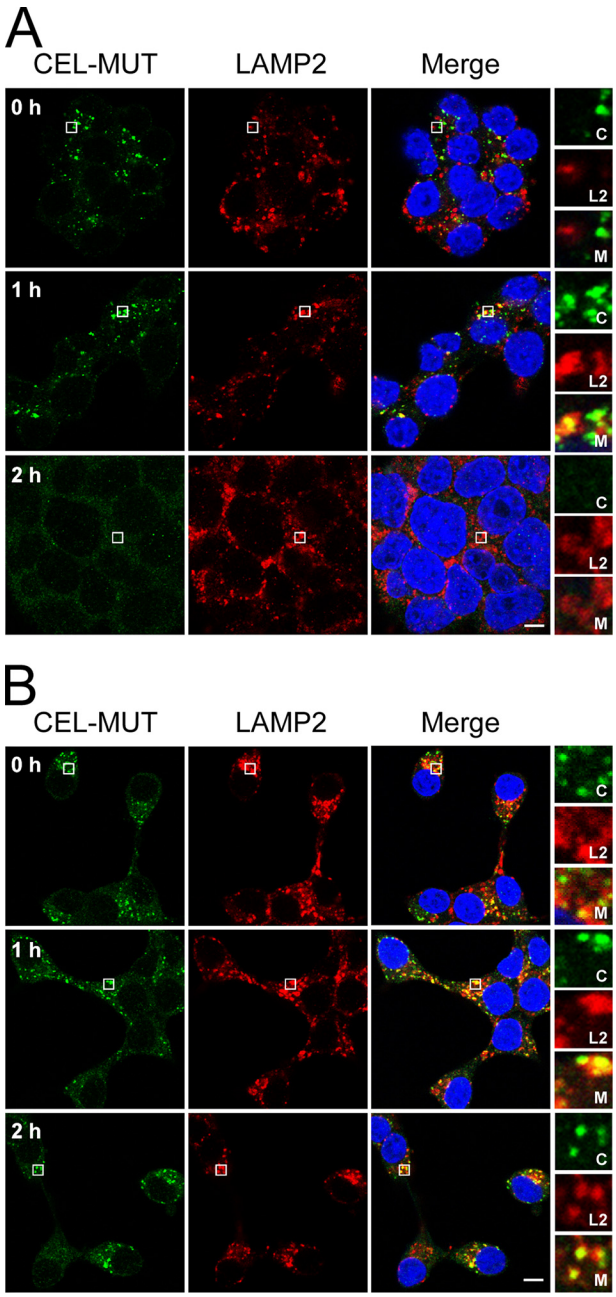

FIGURE 11. **Accumulation in LAMP2-positive vacuoles and degradation of endocytosed CEL-MUT in pancreatic cells.** 266-6 (*A*) and INS 1E (*B*) cells were cultured for 30 min in conditioned medium from HEK293 cells expressing CEL-MUT, washed with PBS, and incubated for the indicated time points (hours) in fresh medium before fixation. The cells were stained using the anti-CEL antibody As20.1 (*green*) and an anti-LAMP2 antibody (*red*). The *insets* show the *boxed areas* in additional 5× magnification. *A*, immediately after the preincubation (*0 h*) CEL-MUT was seen inside most of the 266-6 cells, but none of the CEL-positive vesicles co-localized with LAMP2. At time 1 h, a fraction of the positive vesicles co-localized with LAMP2, whereas 2 h after removal of the conditioned medium the signal from CEL-MUT was lost, indicating that the protein had been degraded. *B*, CEL-MUT-positive vesicles were observed at all time points for the INS 1E cells, and a fraction of these vesicles co-localized with LAMP2. This indicated lysosomal degradation of CEL-MUT in INS 1E cells. The *scale bar* is 5 μm. *C*, CEL; *L2*, LAMP2; *M*, merge.

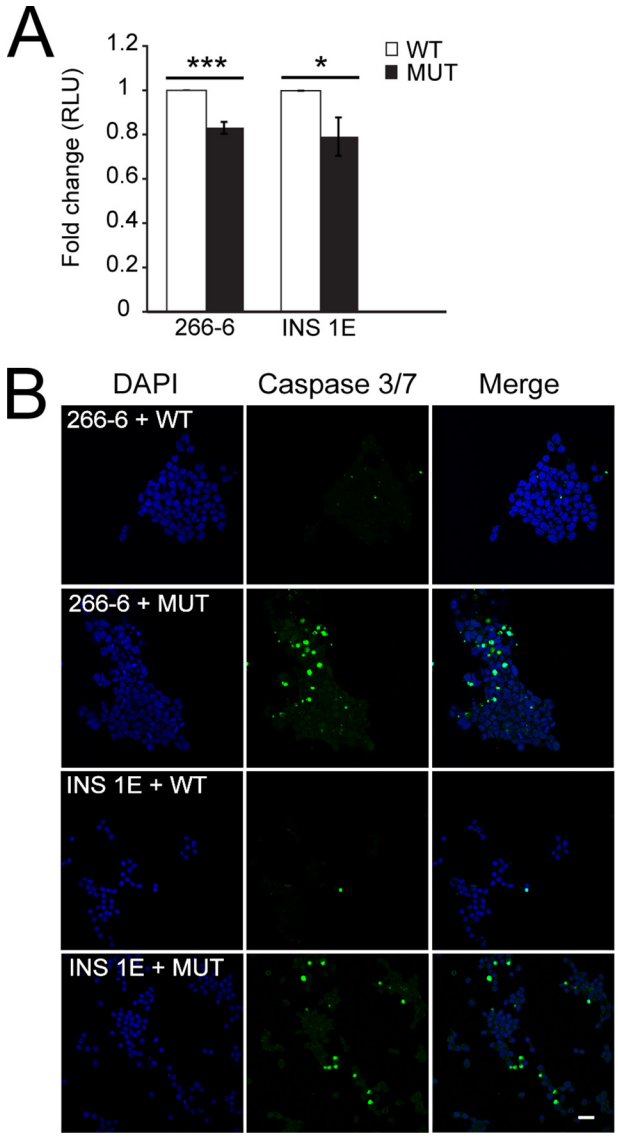

FIGURE 12. **The presence of CEL-MUT reduces the viability of pancreatic cells and increases caspase-3/7 activity.** 266-6 and INS 1E cells were grown for 7 days in the presence of conditioned medium from HEK293 cells stably expressing CEL-WT or CEL-MUT. *A*, cell viability measured as intracellular ATP content. 266-6 and INS 1E cells exposed to CEL-MUT exhibited reduced viability compared with cells exposed to CEL-WT. The experiments were repeated four times, each time with 12 parallels per condition. *Bars* represent S.E. ($n = 4$); * and *** mean $p < 0.05$ and $p < 0.001$, respectively. *RLU*, relative light units. *B*, visualization of caspase-3/7 activity employed to evaluate apoptosis induction. Both 266-6 and INS 1E cells showed elevated caspase-3/7 activity when cultured in medium containing CEL-MUT when compared with CEL-WT exposure. The *scale bar* is 20 μm.

port an active uptake of the protein via endocytosis rather than passive diffusion through the plasma membrane (Fig. 7*C*). The tendency of the protein to aggregate most likely contributes to the increased internalization of the protein as we have observed elongated aggregates on the external side of the plasma membrane by EM (26) (Fig. 2). Moreover, in our immunofluorescence experiments a layer of secreted CEL-MUT was noted covering both the cells and the coverslip, suggesting a "sticky" protein. This phenomenon may be caused by the net charge of CEL-MUT, which is changed from negative to positive due to the new amino acid composition of the VNTR, making the mutant protein more susceptible to interact with negative surfaces such as cell membranes (26).

Spreading of aggregated proteins from cell to cell via the extracellular space has been shown for Alzheimer, Parkinson, and Huntington diseases, demonstrating that protein aggrega-

tion contributes to increased internalization of proteins (for review, see Ref. 43). How the aggregates in these neurodegenerative diseases are released and then taken up again is still under investigation. However, in cultured cells grown in the presence of α-synuclein, a misfolded protein involved in the development of Parkinson disease, internalized α-synuclein aggregates partially co-localized with endosomal and lysosomal markers, implying that the endocytotic machinery is one of the mechanisms involved (44).

The disease-causing properties of CEL-MUT are likely to reside in the C-terminal VNTR domain, which is of a different amino acid composition than in normal CEL. In the latter the addition of *O*-glycans results in increased stability of the protein, as the mucin-like tail protruding from the globular, N-terminal part of the protein appears to protect the enzyme from proteolytic degradation by pancreatic enzymes in the duodenum (16). Our previous studies showed that both CEL-WT and CEL-MUT undergo *O*-glycosylation in HEK293 cells, demonstrating that the changed VNTR of the mutant can act as a substrate for this modification although the sequence is different and the theoretical number of *O*-glycosylation sites is lower than in CEL-WT (26). However, the exact content and composition of the glycans attached to each protein variant has not yet been determined. Even if the glycans were similar, they could have a different impact on the oppositely charged C termini of CEL-MUT and CEL-WT, leading to altered interactions with other molecules.

Interestingly, differences in *O*-glycosylation and VNTR length have recently been shown to change the properties of a CEL protein variant with the same amino acid backbone as CEL-WT. This variant, denoted fetoacinar pancreatic protein (FAPP) has only six repeated segments in its VNTR and was identified in pancreatic ductal adenocarcinomas. Here, the addition of a fucose-rich glycotype within the VNTR domain causes the fetoacinar pancreatic protein to be internalized by dendritic cells, subsequently inducing their maturation (45). As a consequence, the immune system is activated, demonstrating the dramatic effects that can be caused by changes in glycotype within the CEL VNTR (45). The internalization of CEL-MUT might, therefore, also be caused by changes in the glycans attached to the protein. This could involve binding to receptors recognizing specific glycan moieties on the plasma membrane, possibly followed by activation of intracellular processes.

Theoretically, the pathological effects of CEL-MUT could be induced solely by the lack of the normal, highly *O*-glycosylated and mucin-like C terminus of the CEL protein. To test this possibility, we included a truncated protein variant in our experiments. CEL-TRUNC only contained the first four amino acids of the VNTR region and, therefore, lacked most of the C-terminal domain. In previous studies, the CEL VNTR has been suggested to be important for the stability and secretion of this protein; however, not for its catalytic activity (17, 46–48). As CEL-TRUNC in several respects exhibited cellular properties intermediate of CEL-WT and CEL-MUT (Figs. 1 and 7), we conclude that the lack of a normal VNTR sequence may also contribute to the pathological process. In this regard it should be noted that the human *CEL* gene is highly polymorphic and that some variants with very short VNTR sequences exist (20, 24). This calls for studies of such variants as risk factors in pancreatic disease.

CEL is not expressed in cells residing in the islets of Langerhans, an observation that raises the question of why all CEL-MODY patients eventually develop diabetes (24). We have previously hypothesized that the mutant protein is cytotoxic and that this toxicity ultimately leads to acinar cell death and replacement by fibrotic tissue and fat (25, 26). We show here that secreted CEL-MUT is endocytosed by pancreatic cell models (Fig. 10). Moreover, when these cells were exposed to CEL-MUT for 1 week, significantly reduced viability and increased apoptotic activity were observed compared with exposure to the normal protein (Fig. 12). This supports the notion that mutant CEL displays some level of cytotoxicity, and one might further speculate that beta cells are particularly vulnerable in this regard. Thus, studies of the effect of secreted CEL-MUT on human islets *in vitro* are now needed. Alternatively, preparation of induced pluripotent stem cells from patients with CEL-MODY mutations could be an interesting option for further studies (49).

Clinical investigations in our group have demonstrated that, before diabetes development, CEL-MODY patients exhibit severe reduction in pancreatic acinar function and moderate reduction in ductal function (24, 50). Both cystic fibrosis and chronic pancreatitis are conditions associated with a loss of pancreatic endocrine function after the exocrine dysfunction has become manifest. The pathophysiological mechanisms in these syndromes are intricate, involving beta cell failure and destruction secondary to chronic inflammation and fibrosis (51). Notably, a recent study reported an increase in MAPK-driven cytokines in the duodenal juice of CEL-MODY patients (52). Loss of beta cell maintenance signaling from the exocrine tissue may also play a role (53) and could, together with inflammation, augment the postulated direct cytotoxic effect of CEL-MUT on beta cells.

In conclusion, our data demonstrate that extracellular CEL-MUT present on the plasma membrane can be cleared by cell-mediated re-uptake and degradation. This might represent a way of preventing cells from long-time exposure to potentially toxic CEL aggregates. However, we suggest that in CEL-MODY these aggregates or their degradation products eventually cause exocrine pancreatic dysfunction in affected children and adolescents followed by onset of diabetes in adulthood.

Acknowledgment—Confocal imaging was performed at the Molecular Imaging Center, University of Bergen (FUGE platform, Research Council of Norway).

REFERENCES

1. Lombardo, D., Guy, O., and Figarella, C. (1978) Purification and characterization of a carboxyl ester hydrolase from human pancreatic juice. *Biochim. Biophys. Acta* **527,** 142–149
2. Lombardo, D., and Guy, O. (1980) Studies on the substrate specificity of a carboxyl ester hydrolase from human pancreatic juice. II. Action on cholesterol esters and lipid-soluble vitamin esters. *Biochim. Biophys. Acta* **611,** 147–155
3. Roudani, S., Miralles, F., Margotat, A., Escribano, M. J., and Lombardo, D. (1995) Bile salt-dependent lipase transcripts in human fetal tissues. *Biochim. Biophys. Acta* **1264,** 141–150
4. Bläckberg, L., Angquist, K. A., and Hernell, O. (1987) Bile-salt-stimulated

lipase in human milk: evidence for its synthesis in the lactating mammary gland. *FEBS Lett.* **217,** 37–41
5. Lombardo, D., Fauvel, J., and Guy, O. (1980) Studies on the substrate specificity of a carboxyl ester hydrolase from human pancreatic juice. I. Action on carboxyl esters, glycerides, and phospholipids. *Biochim. Biophys. Acta* **611,** 136–146
6. Bernbäck, S., Bläckberg, L., and Hernell, O. (1990) The complete digestion of human milk triacylglycerol *in vitro* requires gastric lipase, pancreatic colipase-dependent lipase, and bile salt-stimulated lipase. *J. Clin. Invest.* **85,** 1221–1226
7. Bruneau, N., Richard, S., Silvy, F., Verine, A., and Lombardo, D. (2003) Lectin-like Ox-LDL receptor is expressed in human INT-407 intestinal cells: involvement in the transcytosis of pancreatic bile salt-dependent lipase. *Mol. Biol. Cell* **14,** 2861–2875
8. Caillol, N., Pasqualini, E., Mas, E., Valette, A., Verine, A., and Lombardo, D. (1997) Pancreatic bile salt-dependent lipase activity in serum of normolipidemic patients. *Lipids* **32,** 1147–1153
9. Comte, B., Franceschi, C., Sadoulet, M. O., Silvy, F., Lafitte, D., Benkoel, L., Nganga, A., Daniel, L., Bernard, J. P., Lombardo, D., and Mas, E. (2006) Detection of bile salt-dependent lipase, a 110-kDa pancreatic protein, in urines of healthy subjects. *Kidney Int.* **69,** 1048–1055
10. Bruneau, N., de la Porte, P. L., Sbarra, V., and Lombardo, D. (1995) Association of bile-salt-dependent lipase with membranes of human pancreatic microsomes. *Eur. J. Biochem.* **233,** 209–218
11. Bruneau, N., and Lombardo, D. (1995) Chaperone function of a Grp 94-related protein for folding and transport of the pancreatic bile salt-dependent lipase. *J. Biol. Chem.* **270,** 13524–13533
12. Bruneau, N., Lombardo, D., Levy, E., and Bendayan, M. (2000) Roles of molecular chaperones in pancreatic secretion and their involvement in intestinal absorption. *Microsc. Res. Tech.* **49,** 329–345
13. Abouakil, N., Mas, E., Bruneau, N., Benajiba, A., and Lombardo, D. (1993) Bile salt-dependent lipase biosynthesis in rat pancreatic AR 4–2 J cells. Essential requirement of *N*-linked oligosaccharide for secretion and expression of a fully active enzyme. *J. Biol. Chem.* **268,** 25755–25763
14. Bruneau, N., Nganga, A., Fisher, E. A., and Lombardo, D. (1997) O-Glycosylation of C-terminal tandem-repeated sequences regulates the secretion of rat pancreatic bile salt-dependent lipase. *J. Biol. Chem.* **272,** 27353–27361
15. Rogers, S., Wells, R., and Rechsteiner, M. (1986) Amino acid sequences common to rapidly degraded proteins: the PEST hypothesis. *Science* **234,** 364–368
16. Loomes, K. M., Senior, H. E., West, P. M., and Roberton, A. M. (1999) Functional protective role for mucin glycosylated repetitive domains. *Eur. J. Biochem.* **266,** 105–111
17. Loomes, K. M., and Senior, H. E. (1997) Bile salt activation of human cholesterol esterase does not require protein dimerisation. *FEBS Lett.* **405,** 369–372
18. Pasqualini, E., Caillol, N., Valette, A., Lloubes, R., Verine, A., and Lombardo, D. (2000) Phosphorylation of the rat pancreatic bile-salt-dependent lipase by casein kinase II is essential for secretion. *Biochem. J.* **345,** 121–128
19. Reue, K., Zambaux, J., Wong, H., Lee, G., Leete, T. H., Ronk, M., Shively, J. E., Sternby, B., Borgström, B., and Ameis, D. (1991) cDNA cloning of carboxyl ester lipase from human pancreas reveals a unique proline-rich repeat unit. *J. Lipid Res.* **32,** 267–276
20. Torsvik, J., Johansson, S., Johansen, A., Ek, J., Minton, J., Ræder, H., Ellard, S., Hattersley, A., Pedersen, O., Hansen, T., Molven, A., and Njølstad, P. R. (2010) Mutations in the VNTR of the carboxyl-ester lipase gene (CEL) are a rare cause of monogenic diabetes. *Hum. Genet.* **127,** 55–64
21. Higuchi, S., Nakamura, Y., and Saito, S. (2002) Characterization of a VNTR polymorphism in the coding region of the CEL gene. *J. Hum. Genet.* **47,** 213–215
22. Lindquist, S., Bläckberg, L., and Hernell, O. (2002) Human bile salt-stimulated lipase has a high frequency of size variation due to a hypervariable region in exon 11. *Eur. J. Biochem.* **269,** 759–767
23. Ragvin, A., Fjeld, K., Weiss, F. U., Torsvik, J., Aghdassi, A., Mayerle, J., Simon, P., Njølstad, P. R., Lerch, M. M., Johansson, S., and Molven, A. (2013) The number of tandem repeats in the carboxyl-ester lipase (CEL) gene as a risk factor in alcoholic and idiopathic chronic pancreatitis. *Pancreatology* **13,** 29–32
24. Ræder, H., Johansson, S., Holm, P. I., Haldorsen, I. S., Mas, E., Sbarra, V., Nermoen, I., Eide, S. A., Grevle, L., Bjørkhaug, L., Sagen, J. V., Aksnes, L., Søvik, O., Lombardo, D., Molven, A., and Njølstad, P. R. (2006) Mutations in the CEL VNTR cause a syndrome of diabetes and pancreatic exocrine dysfunction. *Nat. Genet.* **38,** 54–62
25. Ræder, H., Haldorsen, I. S., Ersland, L., Grüner, R., Taxt, T., Søvik, O., Molven, A., and Njølstad, P. R. (2007) Pancreatic lipomatosis is a structural marker in nondiabetic children with mutations in carboxyl-ester lipase. *Diabetes* **56,** 444–449
26. Johansson, B. B., Torsvik, J., Bjørkhaug, L., Vesterhus, M., Ragvin, A., Tjora, E., Fjeld, K., Hoem, D., Johansson, S., Ræder, H., Lindquist, S., Hernell, O., Cnop, M., Saraste, J., Flatmark, T., Molven, A., and Njølstad, P. R. (2011) Diabetes and pancreatic exocrine dysfunction due to mutations in the carboxyl ester lipase gene-maturity onset diabetes of the young (CEL-MODY): a protein misfolding disease. *J. Biol. Chem.* **286,** 34593–34605
27. Bjørkøy, G., Lamark, T., Brech, A., Outzen, H., Perander, M., Overvatn, A., Stenmark, H., and Johansen, T. (2005) p62/SQSTM1 forms protein aggregates degraded by autophagy and has a protective effect on huntingtin-induced cell death. *J. Cell Biol.* **171,** 603–614
28. Sannerud, R., Marie, M., Nizak, C., Dale, H. A., Pernet-Gallay, K., Perez, F., Goud, B., and Saraste, J. (2006) Rab1 defines a novel pathway connecting the pre-Golgi intermediate compartment with the cell periphery. *Mol. Biol. Cell* **17,** 1514–1526
29. Sannerud, R., Marie, M., Hansen, B. B., and Saraste, J. (2008) Use of polarized PC12 cells to monitor protein localization in the early biosynthetic pathway. *Methods Mol. Biol.* **457,** 253–265
30. McLean, I. W., and Nakane, P. K. (1974) Periodate-lysine-paraformaldehyde fixative. A new fixation for immunoelectron microscopy. *J. Histochem. Cytochem.* **22,** 1077–1083
31. Brown, W. J. (1999) Immunoperoxidase methods for localization of antigens in cultured cells and tissues. Chapter 4 in *Current Protocols in Cell Biology*, John Wiley & Sons, Inc., New York
32. Bruneau, N., Lombardo, D., and Bendayan, M. (1998) Participation of GRP94-related protein in secretion of pancreatic bile salt-dependent lipase and in its internalization by the intestinal epithelium. *J. Cell Sci.* **111,** 2665–2679
33. Ying, M., Flatmark, T., and Saraste, J. (2000) The p58-positive pre-Golgi intermediates consist of distinct subpopulations of particles that show differential binding of COPI and COPII coats and contain vacuolar H^+-ATPase. *J. Cell Sci.* **113,** 3623–3638
34. Rock, K. L., Gramm, C., Rothstein, L., Clark, K., Stein, R., Dick, L., Hwang, D., and Goldberg, A. L. (1994) Inhibitors of the proteasome block the degradation of most cell proteins and the generation of peptides presented on MHC class I molecules. *Cell* **78,** 761–771
35. Yoshimori, T. (2004) Autophagy: a regulated bulk degradation process inside cells. *Biochem. Biophys. Res. Commun.* **313,** 453–458
36. Febbraio, M., and Silverstein, R. L. (1990) Identification and characterization of LAMP-1 as an activation-dependent platelet surface glycoprotein. *J. Biol. Chem.* **265,** 18531–18537
37. Lee, D. H., and Goldberg, A. L. (1998) Proteasome inhibitors: valuable new tools for cell biologists. *Trends Cell Biol.* **8,** 397–403
38. Vesterhus, M., Ræder, H., Kurpad, A. J., Kawamori, D., Molven, A., Kulkarni, R. N., Kahn, C. R., and Njølstad, P. R. (2010) Pancreatic function in carboxyl-ester lipase knockout mice. *Pancreatology* **10,** 467–476
39. Mizushima, N., Yoshimori, T., and Levine, B. (2010) Methods in mammalian autophagy research. *Cell* **140,** 313–326
40. Kouroku, Y., Fujita, E., Tanida, I., Ueno, T., Isoai, A., Kumagai, H., Ogawa, S., Kaufman, R. J., Kominami, E., and Momoi, T. (2007) ER stress (PERK/eIF2α phosphorylation) mediates the polyglutamine-induced LC3 conversion, an essential step for autophagy formation. *Cell Death Differ.* **14,** 230–239
41. Pankiv, S., Clausen, T. H., Lamark, T., Brech, A., Bruun, J. A., Outzen, H., Øvervatn, A., Bjørkøy, G., and Johansen, T. (2007) p62/SQSTM1 binds directly to Atg8/LC3 to facilitate degradation of ubiquitinated protein aggregates by autophagy. *J. Biol. Chem.* **282,** 24131–24145
42. Watanabe, Y., and Tanaka, M. (2011) p62/SQSTM1 in autophagic clear-

ance of a non-ubiquitylated substrate. *J. Cell Sci.* **124,** 2692–2701
43. Brundin, P., Melki, R., and Kopito, R. (2010) Prion-like transmission of protein aggregates in neurodegenerative diseases. *Nat. Rev. Mol. Cell Biol.* **11,** 301–307
44. Lee, H. J., Suk, J. E., Bae, E. J., Lee, J. H., Paik, S. R., and Lee, S. J. (2008) Assembly-dependent endocytosis and clearance of extracellular α-synuclein. *Int. J. Biochem. Cell Biol.* **40,** 1835–1849
45. Franceschi, C., Collignon, A., Isnardon, D., Benkoel, L., Vérine, A., Silvy, F., Bernard, J. P., Lombardo, D., Beraud, E., Olive, D., and Mas, E. (2011) A novel tumor-associated pancreatic glycoprotein is internalized by human dendritic cells and induces their maturation. *J. Immunol.* **186,** 4067–4077
46. Downs, D., Xu, Y. Y., Tang, J., and Wang, C. S. (1994) Proline-rich domain and glycosylation are not essential for the enzymic activity of bile salt-activated lipase. Kinetic studies of T-BAL, a truncated form of the enzyme, expressed in *Escherichia coli*. *Biochemistry* **33,** 7979–7985
47. Hansson, L., Bläckberg, L., Edlund, M., Lundberg, L., Strömqvist, M., and Hernell, O. (1993) Recombinant human milk bile salt-stimulated lipase. Catalytic activity is retained in the absence of glycosylation and the unique proline-rich repeats. *J. Biol. Chem.* **268,** 26692–26698
48. Loomes, K. M. (1995) Structural organisation of human bile-salt-activated lipase probed by limited proteolysis and expression of a recombinant truncated variant. *Eur. J. Biochem.* **230,** 607–613
49. Teo, A. K., Windmueller, R., Johansson, B. B., Dirice, E., Njolstad, P. R., Tjora, E., Ræder, H., and Kulkarni, R. N. (2013) Derivation of human induced pluripotent stem cells from patients with maturity onset diabetes of the young. *J. Biol. Chem.* **288,** 5353–5356
50. Tjora, E., Wathle, G., Engjom, T., Erchinger, F., Molven, A., Aksnes, L., Haldorsen, I. S., Dimcevski, G., Njølstad, P. R., and Ræder, H. (2013) Severe pancreatic dysfunction but compensated nutritional status in monogenic pancreatic disease caused by carboxyl-ester lipase mutations. *Pancreas* **42,** 1078–1084
51. Sasikala, M., Talukdar, R., Pavan kumar, P., Radhika, G., Rao, G. V., Pradeep, R., Subramanyam, C., and Nageshwar Reddy, D. (2012) Beta cell dysfunction in chronic pancreatitis. *Dig. Dis. Sci.* 57, 1764–1772
52. Ræder, H., McAllister, F. E., Tjora, E., Bhatt, S., Haldorsen, I., Hu, J., Willems, S. M., Vesterhus, M., El Ouaamari, A., Liu, M., Ræder, M. B., Immervoll, H., Hoem, D., Dimcevski, G., Njølstad, P. R., Molven, A., Gygi, S. P., and Kulkarni, R. N. (2014) Carboxyl-ester lipase maturity-onset diabetes of the young is associated with development of pancreatic cysts and upregulated MAPK signaling in secretin-stimulated duodenal fluid. *Diabetes* **63,** 259–269
53. Chen, N., Unnikrishnan, I R., Anjana, R. M., Mohan, V., and Pitchumoni, C. S. (2011) The complex exocrine-endocrine relationship and secondary diabetes in exocrine pancreatic disorders. *J. Clin. Gastroenterol.* **45,** 850–861